This is original version of an article whose final and definitive form will be published in Modelling Simul. Mater. Sci. Eng. The article is available online at:
https://iopscience.iop.org/article/10.1088/1361-651X/aaef1a .

On 2D interface networks translation-invariant under curvature-driven migration

A. Morawiec
Polish Academy of Sciences, Institute of Metallurgy and Materials Science
Reymonta 25, 30–059 Kraków, Poland
E-mail: nmmorawi@cyf-kr.edu.pl
Tel.: ++48–122952854 Fax: ++48–122952804

Abstract

The issue of constructing interface networks translating under the curvature driven migration is addressed. The translating networks are the main accessory for testing capillarity driven migration mode in grain growth simulations. They also arise in experimental studies of boundary mobility and junction drag. The networks are constructed of pieces of simple translating curves – lines and Grim Reapers – meeting at triple junctions. The primary method of building the networks relies on a certain property of Grim Reapers which reduces the construction to simple algebraic operations. At the outset, networks of interfaces having different tensions are considered. More detailed discussion concerns a restricted model in which the migration speed does not depend on the tensions. In this second case, the networks have noteworthy properties: some cell dimensions are directly related to angles at triple junctions, there are simple expressions for area sweeping rates, and there is a convenient and elegant alternative way of constructing these particular networks.

Keywords: Grain growth; Interfaces; Triple junctions; Curve shortening flow; Grim Reaper curve;

---

1. Introduction

Grain growth in pure single-phase metals is the 'testing ground' for continuum-based computational methods for simulation of evolution of polycrystalline microstructures [1]. To simplify the problem, many simulations are based on two-dimensional (2D) microstructure models. The grain coarsening is a result of decrease in free energy of grain boundaries via reduction of boundary length [2]. 2D grain boundary networks have the topology of polygonal complexes (plane filling polygons attached edge-to-edge) with three edges meeting at a vertex. Geometrically, the boundaries are non-intersecting curves meeting at triple junctions at angles satisfying equilibrium conditions.

The phenomenon of grain growth has many aspects, but the fundamental one is the kinetics of the boundary motion. In the key model – the so-called capillarity-driven growth, the interface migration speed is proportional to local interface curvature. Before incorporating other aspects of grain growth, credible simulation software is expected to imitate the capillarity-driven boundary migration. Simulation of grain growth is a persistent challenge mainly due to complications at boundary junctions [3–5], and a thorough and constructive testing of the capillarity-driven mode is an essential element of development of simulation software. Simulation algorithms are best validated on boundary networks with theoretically known paths of evolution. Particularly convenient are the networks which remain in steady state, i.e., preserve their shape under the capillarity-driven migration. This paper concerns some networks of this kind, namely networks which move by translation. Simple steady networks have been used in the past [3–8] but their assortment was quite limited, and as was noted in [8], "we need a larger set of analytical benchmarks".

Grain configurations which can be observed for prolonged times without changes of shapes and sizes are also useful in experimental studies of grain growth or measurements of grain boundary properties [9, 10]. In particular, such boundary configurations were applied in research on boundary mobility and on drag caused by boundary junctions; see [11] and references therein. From the experimental perspective crucial is the point that "the steady-state motion of a grain boundary system with a triple junction is only possible in a very narrow range of geometrical boundary configurations" [12]. There is a question how narrow this range really is, and it is interesting to learn more about possible steady configurations.

The 2D model of capillarity-driven grain boundary migration is directly related to the mathematical subject known as the 'curve-shortening flow'. The curve-shortening formalism deals with a smooth planar curve moving in the direction normal to the curve toward its concave side with the speed equal to its local curvature. Some curves migrating in this way remain self-similar [13]. Besides the trivial solution of a static straight line, there are rotating spirals or curves with the property of scaling. From the perspective of grain-growth modeling, most interesting are the curves invariant under translations. Particularly important are compound configurations with curve junctions. Such translating networks of curves flowing by curvature have also been considered in mathematical literature; see, e.g., [14, 15]. However, general mathematical deliberations largely concern existence and uniqueness of flows, whereas developers of simulation software are more interested in explicit and practical descriptions of theoretically supported models.

Moreover, there is a difference between the mathematical curve networks flowing by curvature and the conventional model of capillarity-driven grain growth. Besides the interface curvature, the physical grain boundary migration model involves an additional aspect – the interface tension. The tension, generally different for different interfaces, affects the boundary motion. Within the basic grain growth model, tensions of boundaries meeting at a triple point determine the angles at which they meet, and the speed v of boundary migration is not only proportional to the local curvature κ, but also to the tension σ [2], i.e., one has the tension-weighted curvature flow $v \propto \sigma\kappa$. This kinetic law of boundary migration and the 'curve-shortening flow' can be combined in

$$v = \mu\sigma^M \kappa \ , \tag{1}$$

where M is allowed to take the values of 0 and 1.

With $M = 1$, both the interface speed and the angles depend on tensions ascribed to interfaces. With $M = 0$, the tensions do not affect the speed but they are assumed to determine the angles. If all tensions are equal ($\sigma = \text{const}$), the formula for speed reduces to that of 'curve-shortening flow', and the equilibrium angles between interfaces are $2\pi/3$; this approach is known as the "uniform boundary model" or UBM [16]. Only these three cases are considered below. Generally, the interface tension is a tensorial quantity [17, 18], but in this note, tensions are assumed isotropic and numerically equal to free energy densities. Moreover, the mobilities μ of particular boundaries may differ [2], but here the coefficient μ is assumed to be constant.

We begin with a brief reminder of 2D translating curves. In passing, we set forth our notation, and we introduce a property of 2D translating curves which reduces the construction of curve junctions with prescribed angles to simple algebraic operations. The property is first used to characterize boundaries in tricrystals with equilibrated triple junctions and migration speed affected by tensions ($M = 1$). Then we show how to construct more complicated translating networks, with numerous cells and a diversity of shapes. Details are given for what we call an extended ⋒-shaped configuration. Construction of other translating networks is only outlined as it can be performed in a similar way.

The second part of the paper is devoted to the case of tension-independent speed of migration ($M = 0$). As in the experimental works on junction drag [11, 12, 19], the angles between interfaces at triple points may differ from $2\pi/3$. These translating networks turn out to have interesting geometry with some cell dimensions linked to angles between interfaces at triple points in a simple manner. They implicate expressions for rates of areas swept by the migrating networks. Finally, there is an alternative way of constructing these networks based on a conformal transformation. Results of this part are also applicable to networks within UBM with constant σ and all interface angles equal to $2\pi/3$.

2. The Grim Reaper curve

The structures described below are based on a specific curve migrating by translation introduced by Mullins [20]. It is assumed that the curve is a graph of a real-valued smooth function $y = y(x)$. With $\kappa = \kappa(x)$ representing the signed curvature at x, $v = v(x)$ being the speed of the curvature-driven migration and V denoting the constant non-zero speed of the curve displacement along the ordinate axis, one has

$$v/V = \left(1 + y_x^2\right)^{-1/2} \ ,$$

where y_x is the derivative of y with respect to x and the argument is omitted. Based on (1) and $\kappa = -y_{xx}/\left(1 + y_x^2\right)^{3/2}$, one gets the differential equation

$$y_{xx} + c(1 + y_x^2) = 0 \ , \tag{2}$$

where $c = V/(\mu\sigma^M)$. The equation is satisfied by

$$y(x) = Y + c^{-1} \log\left(\cos\left(c(x - X)\right)\right) \ . \tag{3}$$

The graph of this periodic function consists of U-shaped branches with extrema at $(x, y) = (X + 2k\pi/c, Y)$, where k is an integer. We are interested in a single branch contained in the $\pi/|c|$-wide strip centered at $x = X$. The (assumed to be positive) constant c will be used interchangeably with the width $w = \pi/c$. See Fig. 1. The particular curve $\log\cos x$ is known as the Grim Reaper (GR) [21]. This name will also be used in reference to its (X, Y)-translated and c-scaled apparitions given by (3). The GR curves are steady under curvature driven migration. Another curve with this property is the straight line along the direction of migration. Physically, an individual GR or a straight line represent particular interfaces separating two grains of a 2D bicrystal.

For describing interfaces meeting at a triple point, it is convenient to assume that the junction is at $(x, y) = (0, 0)$. The expression for a GR through $(0, 0)$ such that $\lim_{x\to\beta} y(x) =$

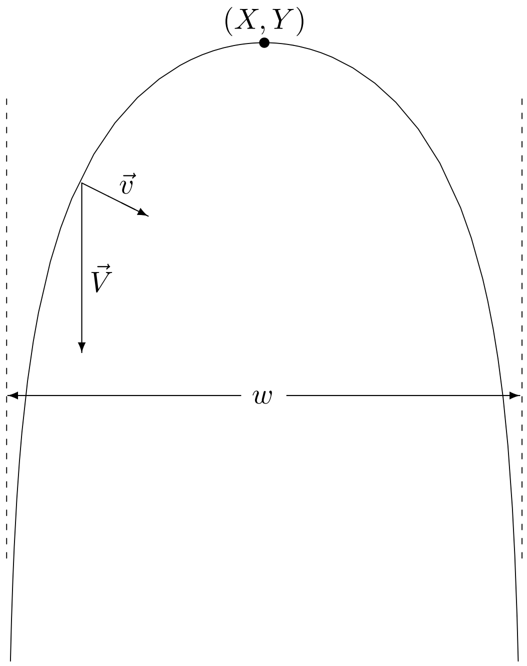

Figure 1: The Grim Reaper curve of width $w = \pi/c$. The symbol $\vec{v}$ denotes the velocity of the curvature-driven migration, and $\vec{V}$ is the velocity of the curve displacement.

$-\infty$ has the form

$$y(x) = f(x;\, c, \beta) = c^{-1} \log \left(\csc(c\beta)\, \sin(c(\beta - x)) \right) \ ,$$

where $0 < |\beta| < w$. If $\beta = b$ is negative, i.e., it corresponds to the left asymptote, the right asymptote is at $\beta = b + w$, and $f(x; c, b + w) = f(x; c, b)$. The position of the GR curve through $(0, 0)$ is determined by unique b in the open interval $(-w, 0)$. Below, we use both b and β for specifying interfaces; in the latter case, we take $\beta = b < 0$ if the piece of the GR forming an interface is to the left to the ordinate axis, and $\beta = b + w > 0$ if it is to the right to the axis. The coordinates of the maximum of $f(x; c, b)$ are

$$(X, Y) = \left(b + w/2,\ c^{-1} \log \left(-\csc(bc) \right) \right) \ . \tag{4}$$

With $\beta \to 0$, the ordinate Y of the GR's maximum tends to infinity, and the curve near $(0, 0)$ comes close to the straight vertical line. Therefore, in the description of interfaces below, β is in the interval $(-w, +w)$, with special interpretation of the corresponding curve when β equals 0: in this case, the interface is a vertical half-line.

GR intersection angle

Before proceeding to the next section, we need to consider the angle of intersection between two GRs migrating in the same direction. The angle is can be expressed by parameters of

GRs using the observation that the integrated curvature $\int \kappa$ of a piece of a GR with abscissa between x_1 and x_2 equals $c(x_2 - x_1)$. This follows directly from (2). Let us now consider a cell between two interfaces described by $f(x; c_L, \beta_L)$ and $f(x; c_R, \beta_R)$. With $\beta_L < \beta_R$, the integrated curvature of the interfaces equals $c_R\,\beta_R - c_L\,\beta_L$. The total curvature of the cell boundary equals π, and it is the sum of the integrated curvature and the curvature $\pi - \theta$ accumulated at the cell vertex with internal angle θ. Hence, one has

$$\theta = c_R\,\beta_R - c_L\,\beta_L \ . \tag{5}$$

If the intersecting GRs have the same widths, i.e., $c_R = c_L = c$, the intersection angle depends only on the distance between symmetry axes of the GRs, i.e., a translation of one of the GRs along its axis does not change the angle (Fig. 2). The expression (5) is convenient for getting geometric parameters of structures built of pieces of GRs intersecting under prescribed angles.

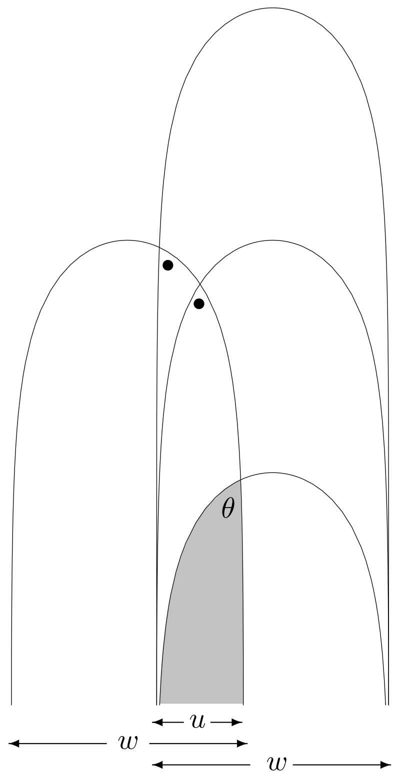

Figure 2: Illustration of the property of intersecting GRs of the same width $w = \pi/c$: the intersection angles marked by disks are equal to $\theta = cu$.

3. Networks of translating interfaces

For a network of pieces of GRs to migrate by translation, the individual GR curves must have parallel symmetry axes and the same speed V. With $M = 1$, the equality of the speeds implies that the product σc is the same for all GRs. In other words, the widths of individual GRs contributing to the network are proportional to tensions ascribed to the corresponding interfaces.

A connected translating network of Grim Reapers and half-lines will be referred to as 'Grim Reaper troop' or GRT. Without limiting generality, the widths of GRs in a GRT can be seen as multiples of a certain scaling factor. The size of the GRT can be changed by changing the scaling factor. The sizes of GRTs in figures below have been chosen for clarity, and scales of figures are not the same.

We begin with considering translating boundaries in tricrystals – three grains separated by three interfaces. These interfaces constitute a simple translating triod [14] with rays meeting under equilibrium conditions.

Young equilibrium conditions and angles at triple points

Let σ_i $(i = 1, 2, 3)$ be the tensions of three interfaces meeting at a junction, and let the inequalities

$$0 < \sigma_i < \sigma_j + \sigma_k \tag{6}$$

hold for all i and $j \neq k$. Let θ_i $(0 < \theta_i < \pi)$ be the angle between interfaces j and k, where $i \neq j \neq k \neq i$. Equilibrium of tensions at the junction is described by Young conditions

$$\sin(\theta_1)/\sigma_1 = \sin(\theta_2)/\sigma_2 = \sin(\theta_3)/\sigma_3 \ .$$

Hence, the angles are determined by tension ratios

$$\cos\theta_i = \frac{\sigma_i^2 - \sigma_j^2 - \sigma_k^2}{2\sigma_j\sigma_k} \ ,$$

and the ratios can be obtained from the angles using $\sigma_i/g_s = 1 - \cot(\theta_j/2)\cot(\theta_k/2)$, where $g_s = \sum_k \sigma_k/2$. Near the bounds (6), when $\sigma_i \to 0$, then $\theta_i \to \pi$, and when $\sigma_i \to \sigma_j + \sigma_k$, then $(\theta_i, \theta_j, \theta_k) \to (0, \pi, \pi)$.

$\cap\!\cap$-*shaped GRT*

Let us consider the junction of three interfaces, each being a piece of a GR. The convention here is that the middle (or inner) interface is denoted by 1 and the outer right and left interfaces are denoted by 2 and 3, respectively. See Fig. 3. Explicitly, the interfaces are described by

$$\begin{aligned}
&f(x; c_1, \beta_1) \quad \text{with} \quad \min(\beta_1, 0) < x < \max(\beta_1, 0) \ , \\
&f(x; c_2, \beta_2) \quad \text{with} \quad 0 < x < \beta_2 \ , \\
&f(x; c_3, \beta_3) \quad \text{with} \quad \beta_3 < x < 0 \ ,
\end{aligned}$$

where c_i are related to tensions via $\sigma_1 c_1 = \sigma_2 c_2 = \sigma_3 c_3$ implied by the equality of migration rates of the GRs. Application of the formula (5) for GR intersection angle leads to

$$\begin{aligned} \theta_1 &= 2\pi - c_2\beta_2 + c_3\beta_3 \ , \\ \theta_2 &= c_1\beta_1 - c_3\beta_3 \ , \\ \theta_3 &= -c_1\beta_1 + c_2\beta_2 \ . \end{aligned} \tag{7}$$

These relationships remain valid if the interface 1 is a half-line along the direction of flow with β_1 equal to zero. With this provision, the above described triod will be referred to as $\Cap$-shaped GRT.

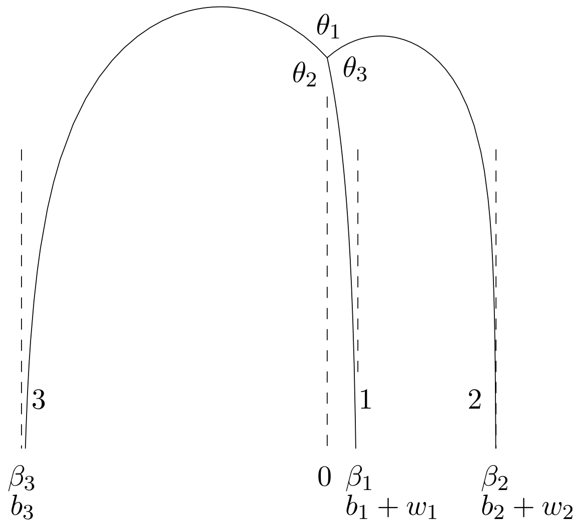

Figure 3: Example $\Cap$-shaped triod for $(\sigma_1, \sigma_2, \sigma_3) \propto (w_1, w_2, w_3) \propto \big(2, 1, \sqrt{3}\big)$. The corresponding angles are $(\theta_1, \theta_2, \theta_3) = (3, 5, 4)\,\pi/6$. The value of $c_1\beta_1$ is $\pi/15$.

To avoid interface intersections, there must occur

$$\beta_3 < \beta_1 < \beta_2 \ . \tag{8}$$

For given angles θ_i, the positions β_i are given by (7), but since these relationships are not independent ($\sum_i \theta_i = 2\pi$), one parameter – let it be β_1 – remains free. Thus, the interface tensions do not fully determine the geometry of the $\Cap$-shaped GRT. One has a one-parameter family of configurations with the shapes of cells depending on the orientation of lines tangent to interfaces at the junction. (For brevity, we will call it "orientation of the junction".) By fixing β_1, a unique configuration is selected. See Fig. 4. With $c_2\beta_2 < \pi$ and $c_3\beta_3 > -\pi$, one has

$$\theta_2 - \pi < c_1\beta_1 < \pi - \theta_3 \ . \tag{9}$$

The closer $c_1\beta_1$ to the lower (upper) bound the closer the interface 3 (2) near the junction to a vertical half-line.

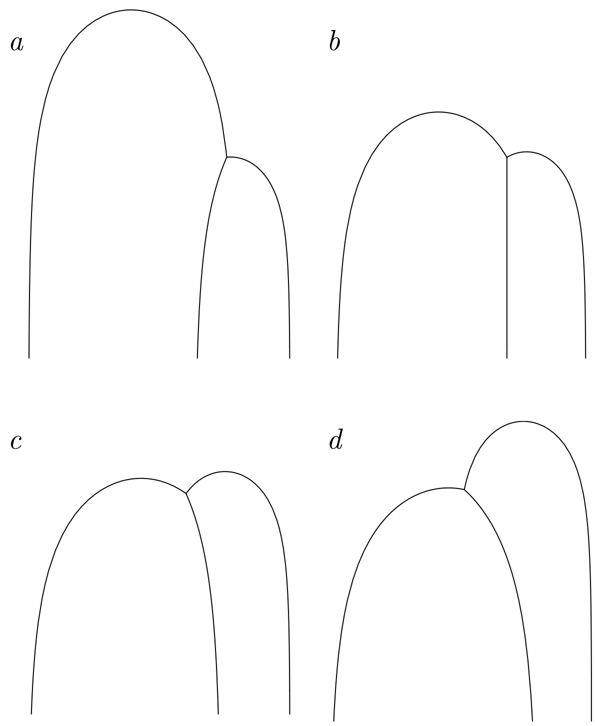

Figure 4: Family of configurations for the same parameters as the GRT in Fig. 3 except $c_1\beta_1$ which equals $-2\pi/15$ in (a), 0 in (b), $2\pi/15$ in (c) and $4\pi/15$ in (d).

The sharper of the inequalities (8) and (9) determine the actual bounds on β_1. The full range of $c_1\beta_1$ given by the difference between the upper and lower bounds is also the range of possible orientations of the junction. Violation of the conditions (8) is illustrated in Fig. 5, and with $c_1\beta_1$ reaching one of the bounds (9) one gets a triod which will be referred to as (inverted) Y GRT.

Inverted Y *configuration*

We consider the case of $\beta_3 \to -w_3$, i.e., $c_1\beta_1$ approaching the lower of limits (9). When the limit is reached, the interface 3 is a vertical half-line. The GR-based left and right interfaces are 1 and 2, respectively, i.e., $b_1 = \beta_1 < 0 < \beta_2 = b_2 + w_2$. The relationships between β_1 and β_2 and the angles θ_i are the same as (7) with $c_3\beta_3$ replaced by $-\pi$. Clearly, since the position of the interface 3 is fixed, the orientation of the junction is established, i.e., the interface tensions uniquely determine the Y-shaped configuration.

Example Y-shaped GRTs are shown in Fig. 6. With $\sigma_1 = \sigma_2$, one has the symmetric configuration used in studies of junction drag; see, e.g., [19]. Another interesting option is $\sigma_2 \to 0$ and $\theta_2 \to \pi$ shown in Fig. 6b. Configurations of this type correspond to the so-called "quarter-loop geometry" used to estimate grain boundary mobility in bicrystal specimens; see, e.g., [10].

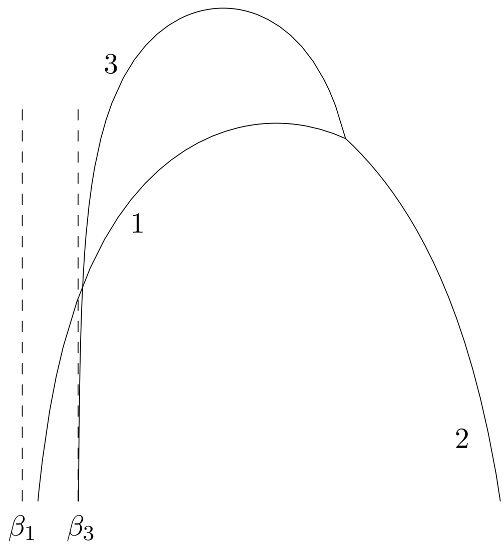

Figure 5: Example configuration illustrating violation of conditions (8). The parameters of the GRT are $(\sigma_1, \sigma_2, \sigma_3) \propto (w_1, w_2, w_3) \propto (7, 10, 4)$ and $c_1\beta_1 = -2$.

Extended $\Cap$-shaped GRT

An $\Cap$-shaped GRT can be used to construct configurations consisting of a larger number of interfaces and junctions. A given structure is naturally enlarged by adding a new junction located on one of the interfaces. As an illustration, the simple case of *extended* $\Cap$-shaped GRTs constructed by adding new junctions on *outermost* interfaces will be considered in details. Their junctions as vertices and bounded[1] interfaces as edges form a path graph.

Below, we use the same conventions for interface designation as above plus an additional bracketed index (n) indicating the junction to which a given entity belongs ($n = 1, \ldots, N$), e.g., the interfaces of the (n)-th junction are $1^{(n)}$, $2^{(n)}$ and $3^{(n)}$, and $\sigma_i^{(n)}$ is the tension of the i-th interface of the (n)-th junction. Given $\sigma_i^{(n)}$ for $n = 1, \ldots, N$, $i = 1, 2, 3$, one also has the parameters $c_i^{(n)}$ and the angles $\theta_i^{(n)}$.

Let the extension of an $\Cap$-shaped GRT be to the right with the GR forming the interface $2^{(n-1)}$ identified with the GR of the interface $3^{(n)}$ ($n = 2, 3, \ldots, N$). Clearly, the interface tensions (and the widths of the GRs) need to be equal

$$\sigma_3^{(n)} = \sigma_2^{(n-1)} \ . \tag{10}$$

Moreover, for the junction (n) to be to the right of the junction $(n-1)$ on a GR, there must occur

$$b_3^{(n)} < b_2^{(n-1)} \ .$$

The structure with N junctions is constructed iteratively: The first step is to get the geomet-

[1]A bounded interface (or a bounded cell) consists of points which are within finite distance of each other.

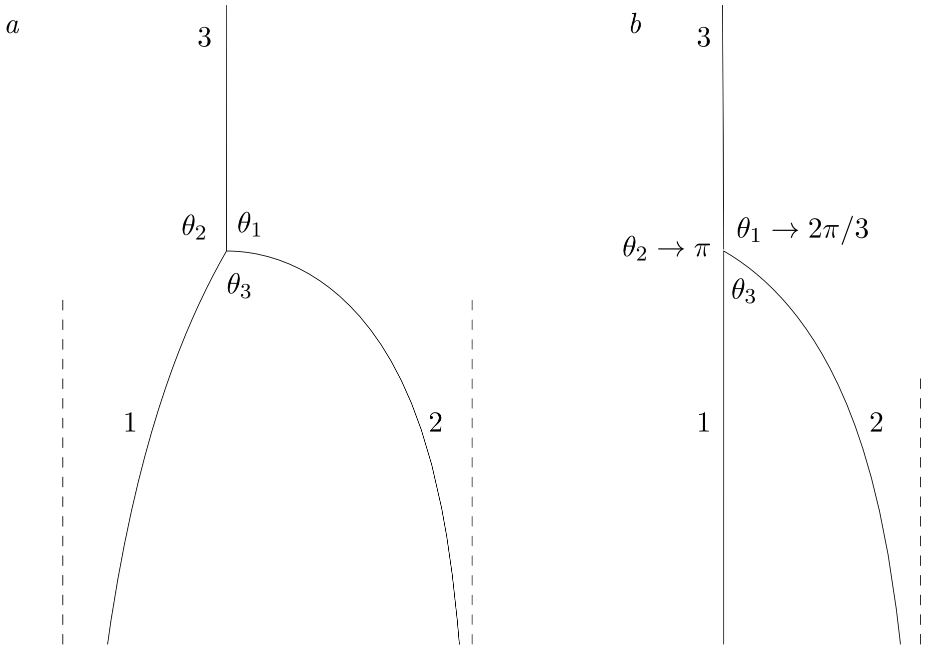

Figure 6: Inverted Y-shaped GRTs. (a) For the same parameters as the GRT in Fig. 3 except $c_1\beta_1$ is which in this case approached $\theta_2 - \pi = -\pi/6$, i.e., the low limit in (9). (b) For $(\sigma_1, \sigma_2, \sigma_3) \propto (1, \epsilon, 1 + \epsilon/2)$ with $\epsilon \to 0$ and $(\theta_1, \theta_2, \theta_3) \to (2, 3, 1)\,\pi/3$.

ric parameters of the interface triod of junction (1) located at $(0, 0)$. Having the structure based on junctions (1)–$(n-1)$, one needs to add the part corresponding to the junction (n). Again, the geometric parameters of the junction (n) are obtained with the junction initially located at $(0, 0)$. This structure is then appended to the known structure of (1)–$(n-1)$ junctions in such a way that the GR of the interface $2^{(n-1)}$ overlaps with the GR of the interface $3^{(n)}$. To this end, the junction (n) with its interfaces is translated from $(0, 0)$ by the vector

$$\mathbf{t}^{(n)} = \mathbf{t}^{(n-1)} + \mathbf{p}_2^{(n-1)} - \mathbf{p}_3^{(n)} ,$$

where $\mathbf{p}_i^{(n)} = \left(X_i^{(n)}, Y_i^{(n)}\right)$ is the position of the maximum of the GR representing the interface $i^{(n)}$ given by (4), $i = 2, 3$, $n = 2, 3, \ldots, N$ and $\mathbf{t}^{(1)} = (0, 0)$. The final (i.e., translated) positions of the maxima and junctions are used to get the domains of individual interfaces. In the process, one needs to check whether there are no intersections of the unbounded interfaces, i.e., whether the inequalities

$$\beta_3^{(1)} < \beta_1^{(1)} , \quad \beta_1^{(n-1)} - X_2^{(n-1)} < \beta_1^{(n)} - X_3^{(n)} \ \ (n = 2, 3, \ldots, N) , \quad \beta_1^{(N)} < \beta_2^{(N)}$$

are satisfied. They replace the conditions (8) used for single-junction ⋒-shaped GRT. The procedure is stopped after the N-th junction is appended.

The construction of extended ⋒-shaped GRTs is illustrated in Fig. 7. This and other

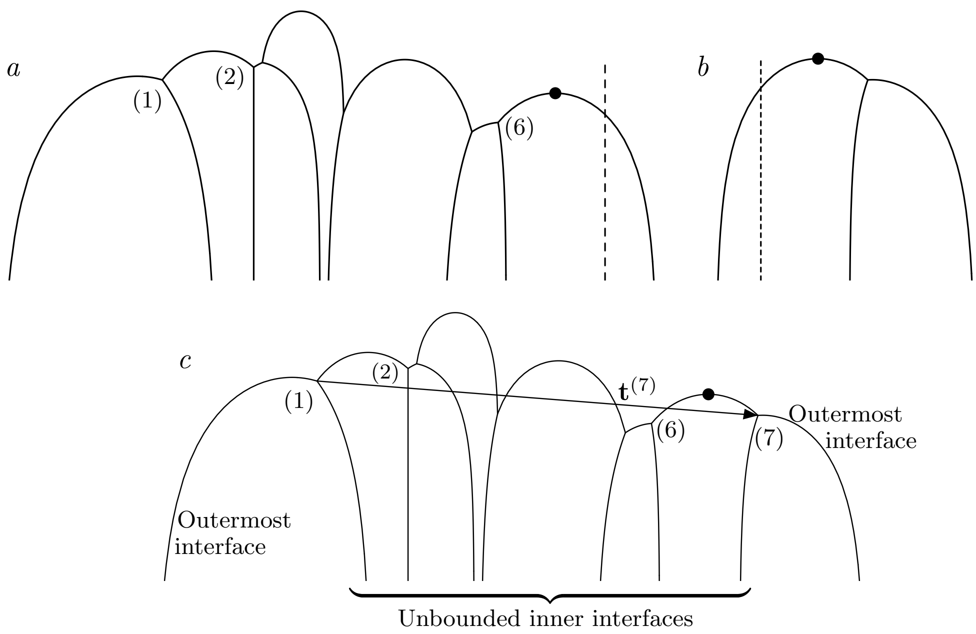

Figure 7: Schematic illustration of the construction of extended $\Cap$-shaped networks. The extended six-junction $\Cap$-shaped GRT shown in (a) is appended with the $\Cap$-shaped troid (b) by translating the latter so the maxima marked by disks overlap. The resulting extended $\Cap$-shaped GRT (c) has seven junctions.

figures with GRTs except Fig. 16 are drawn using a Mathematica code based on the above formulas.

Periodic $\Cap$-shaped GRTs

Like the network in Fig. 7, an extended $\Cap$-shaped GRT can be ended by two outermost GRs. ('Walls' like the one in Fig. 6b are a similar type of ending.) In contrast, typical structures used in testing of simulation algorithms are periodic. They are constructed by repeating a unit element containing N_u (≥ 1) junctions. See Fig. 8a. In our notation, periodicity of an extended $\Cap$-shaped GRT means that $\sigma_i^{(n)} = \sigma_i^{(n+N_u)}$ and $\beta_1^{(n)} = \beta_1^{(n+N_u)}$ for arbitrary integer n. Typically $N_u = 1$ is used; e.g., [3,5]. In this case, the above condition and (10) imply that $\sigma_i^{(n)}$ have the same value for all n and $i = 2, 3$, and $\beta_1^{(n)}$ have the same value for all n. Example periodic network of this kind is shown in Fig. 8b.

Other structures of similar kind are obtained by adding a reflection with respect to a line parallel to the migration direction and passing through a junction or through a maximum of a GR. The simplest network of the second type (mirror line through the maximum) built of an element with a single junction is illustrated in Fig. 8c. (See also [4].)

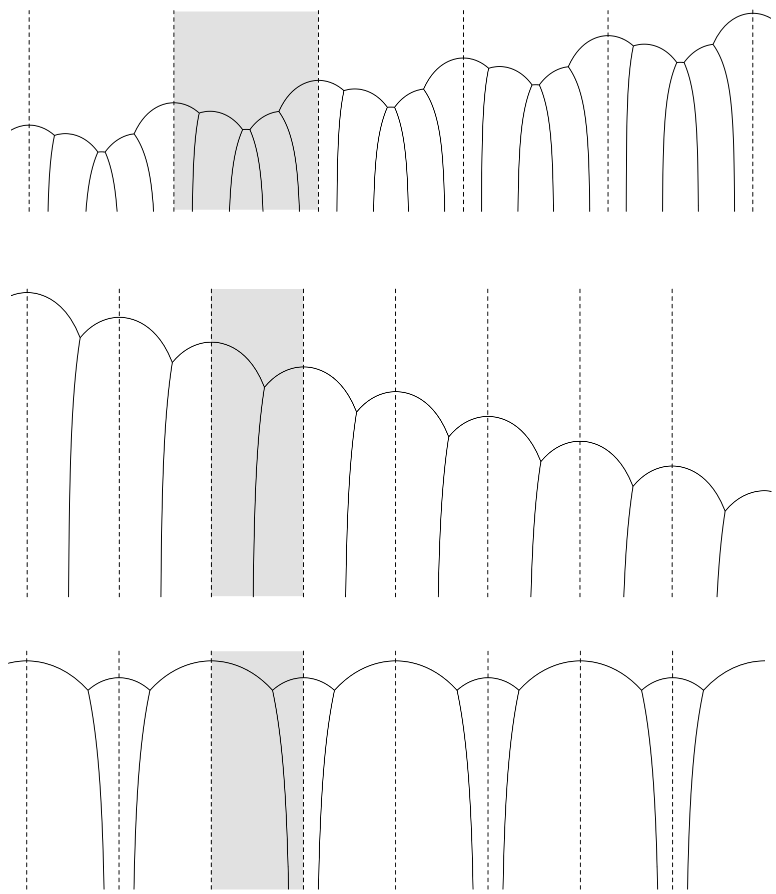

Figure 8: (a) Example periodic network for $N_u = 4$. (b) A periodic network for $N_u = 1$, $(\sigma_1, \sigma_2, \sigma_3) \propto (w_1, w_2, w_3) \propto \left(\sqrt{3}, 1, 1\right)$. The corresponding angles are $(\theta_1, \theta_2, \theta_3) = (2, 5, 5)\,\pi/6$. The value of $c_1\beta_1$ is $-\pi/20$. (c) A network with reflection, $N_u = 1$, the period of $2N_u = 2$, and the parameters of an individual triod as in Fig. 3.

More complex networks

An extended $\sqcap\!\sqcap$-shaped GRT can be enlarged by adding new junctions on its unbounded inner interfaces. The construction is analogous to that of the extended $\sqcap\!\sqcap$-shaped GRTs. The GR forming the interface k_p of the predecessor junction (n_p) needs to be identified with the GR of the interface k_s of the successor junction (n_s). Clearly, tensions of these interfaces need to be equal, i.e., $\sigma_{k_s}^{(n_s)} = \sigma_{k_p}^{(n_p)}$. The junction (n_s) is translated by the vector $\mathbf{t}^{(n_s)} = \mathbf{t}^{(n_p)} + \mathbf{p}_{k_p}^{(n_p)} - \mathbf{p}_{k_s}^{(n_s)}$, where $\mathbf{p}_i^{(n)} = \left(X_i^{(n)},\, Y_i^{(n)}\right)$ is the position of the maximum of the interface $i^{(n)}$ given by eq.(4). Interfaces of an N-sided bounded cell satisfy the closing condition: The GR forming the interface k_p of the last junction (N) is identified with the GR of the interface k_s of the first junction (1), their interface tensions are equal $\sigma_{k_s}^{(1)} = \sigma_{k_p}^{(N)}$, and $\mathbf{t}^{(N)} + \mathbf{p}_{k_p}^{(N)} - \mathbf{p}_{k_s}^{(1)} = \mathbf{0}$. These structures and GRTs containing Y-shaped junctions will be illustrated below for networks involving GRs of the same width.

4. Networks built of GRs of the same width

Translating networks have remarkable properties when they satisfy constraints imposed by UBM. Some of these properties are also relevant in the more general setting with same-width GRs and the angles different from $2\pi/3$. Therefore, the case of $M = 0$ is considered. Results corresponding to UBM are obtained by fixing the angles at $2\pi/3$.

With the speed of migration independent of tension, the widths of all GRs of a given GRT are equal. Formally, since such GRs, and in consequence the GRT, are scaled by $w = \pi/c$, one could confine the derivations to unit c. Below, however, to facilitate practical applications, the coefficient c is retained.

$\Cap$-shaped GRT

For brevity, the distance between asymptotes of infinite-length boundaries of an unbounded cell will be referred to as the 'asymptotic cell width' or briefly the 'cell width'. With $c_1 = c_2 = c_3 = c$, it follows from (7) that the asymptotic widths $d_1 = \beta_1 - \beta_3$ and $d_2 = \beta_2 - \beta_1$ of cells of a $\Cap$-shaped GRT and its total width $D = d_1 + d_2$ are directly related to the angles

$$cD = 2\pi - \theta_1 \ , \quad cd_1 = \theta_2 \ , \quad cd_2 = \theta_3 \ . \tag{11}$$

The rate c and the widths d_n ($n = 1, 2$) determine the angles. On the other hand, given the migration rate and the angles θ_i, the widths of cells are determined, but the position β_1 of the inner interface remains free. Thus, there is a one-parameter family of configurations with the same widths d_n and D but with the shapes of cells depending on the orientation of the junction.

With three GRs of the same width, the condition (8) reflects only the convention used for numbering the interfaces, i.e., differently than in section 3, it does not limit the possible orientations of the junction. The parameter β_1 is limited only by eq.(9). Thus, the full range of $c\beta_1$ is $(\pi - \theta_3) - (\theta_2 - \pi) = \theta_1$, i.e., the range of orientations is θ_1.

Extended $\Cap$-shaped GRT

The relationships (11) can be easily generalized to extended $\Cap$-shaped GRTs. Let d_1 and d_{N+1} be the widths of the outermost cells, and let d_n ($n = 2, \ldots, N$) denote the width of the n-th cell with vertices at the junctions $(n-1)$ and (n). Based on the property of intersecting GRs, the curvature integrated over the interfaces of the n-th cell equals

$$\int \kappa = cd_n \ . \tag{12}$$

The total curvature of the cell boundary is the sum of $\int \kappa$ and the angles supplementary to the internal angles of the cell. Hence, with $\theta_3^{(0)} = \pi = \theta_2^{(N+1)}$, one has

$$cd_n = \theta_3^{(n-1)} + \theta_2^{(n)} - \pi \ , \tag{13}$$

where $n = 1, \ldots, N+1$. Thus, for a given migration rate, the angles $\theta_i^{(n)}$ determine the widths of the cells. Since the positions $\beta_1^{(n)}$ of the inner interfaces remain free, there are translating networks having the same rate c, the same sets of angles $\theta_i^{(n)}$ $(n = 1, \ldots, N)$ and cell widths d_n $(n = 1, \ldots, N+1)$ but different shapes[2]; see Fig. 9.

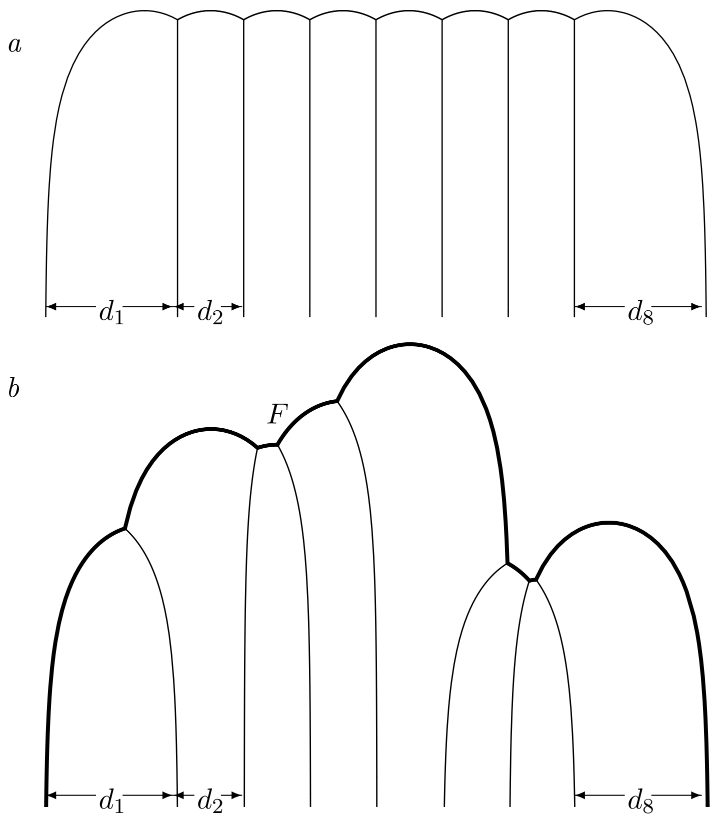

Figure 9: Two extended ⋒-shaped configurations for UBM. In (a), all $\beta_1^{(n)}$ are 0, i.e., all internal interfaces are straight. In (b), the parameters $\beta_1^{(n)}$ are chosen randomly within the constraints (9). The asymptotic cell widths d_n in (b) are the same as in (a). The thicker curve in (b) marks the front F.

Let F denote the 'front' of migration of an extended ⋒-shaped GRT, i.e., the path linking the triple points plus two outermost interfaces (Fig. 9). Summation of (12) over n gives the curvature integrated over F (as the integrals over common interfaces of neighboring

[2] On the other hand, given c and the widths d_n $(n = 1, \ldots, N+1)$, there are $N+1$ conditions on $2N$ independent angles $\theta_i^{(n)}$, i.e., there are $N-1$ free parameters. Thus, only in the case of one junction, the rate c and widths d_n of the cells determine the angles.

cells are canceled out). Hence, one has

$$\int_F \kappa = \sum_{n=1}^{N+1} c\, d_n = cD \ ,$$

where $D = \sum_{n=1}^{N+1} d_n$ is the total width of the extended $\Cap$-shaped GRT. Using the property of intersecting GRs, one gets $cD + \sum_{n=1}^{N}(\theta_1^{(n)} - \pi) = \pi$. Thus, for a given c, the total width D is determined by the sum $\sum_{n=1}^{N} \theta_1^{(n)}$ of the angles opposite to the unbounded inner interfaces. The term cD is directly linked to the time derivative $\dot{A}$ of the area A swept by the front F: $\dot{A} = DV = \mu cD$. Hence, one has

$$cD = \dot{A}/\mu = (N+1)\pi - \sum_{n=1}^{N} \theta_1^{(n)} \ .$$

In particular, if tensions are all equal, all $\theta_i^{(n)}$ are $2\pi/3$, the outermost cells have the widths $d_1 = 2w/3 = d_{N+1}$, the widths of inner cells are all $d_n = w/3$ ($n = 2, \ldots, N$), and the total width D of the structure and the sweeping rate are given by $cD = \dot{A}/\mu = (N+3)\pi/3$.

GRTs with Y*-shaped triods*

One may also consider structures similar to extended $\Cap$-shaped GRTs (multi-junction, path-based, with unbounded inner interfaces), but with some straight interfaces directed up, i.e., GRTs involving both $\Cap$-shaped and Y-shaped junction configurations; see Fig. 10. Similarly to eq. (13), the relationships between the widths of other cells and angles follow form (5). In the case of a single triple point and Y-shaped configuration, the width $D = \beta_2 - \beta_1$ of the cell between interfaces 1 and 2 is related to the θ_3 angle via $cD = \theta_3$. If the number of triple points is N, and N_{Y} is the number of Y-type junctions, then $\int_F \kappa - \sum_{n=1}^{N} p_n \left(\pi - \theta^{(n)}\right) = \pi$ or

$$cD = \dot{A}/\mu = (N - 2N_{\mathsf{Y}} + 1)\pi - \sum_{n=1}^{N} p_n \theta^{(n)} \ ,$$

where $p_n = +1$, $\theta^{(n)} = \theta_1^{(n)}$ if the unbounded inner interface at the junction (n) is directed down, and $p_n = -1$, $\theta^{(n)} = \theta_3^{(n)}$ if it is directed up. Thus, the width of the structure and the rate of sweeping the area are determined by the angles $\theta^{(n)}$.

In the case of UBM, the above expression takes the form $cD = \dot{A}/\mu = (N - 2N_{\mathsf{Y}} + 3)\,\pi/3$. The widths of cells below the front F are 0, $w/3$ and $2w/3$. The widths of cells above the front are multiples of $w/3$, and so are the distances between half-lines above the front and the asymptotes of GRs.

Tree-like structures

Other configurations can be constructed by developing the lower parts of GRTs described

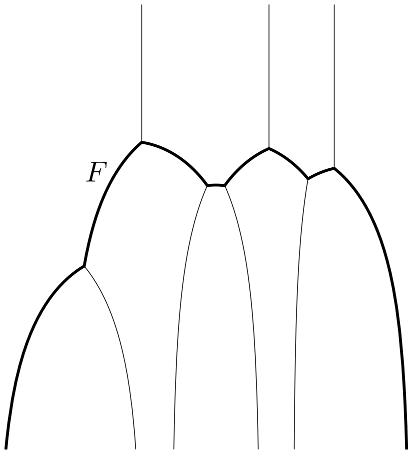

Figure 10: Example GRT with Y-shaped triods. The thicker curve marks the front F.

above: the interface $1^{(n_p)}$ of such a GRT is identified with either interface $2^{(n_s)}$ or $3^{(n_s)}$ of an additional triod. In such cases, the total width of the structure and the area swept by it are not affected. An example GRT of this kind is in Fig. 11. The figure also shows that a GRT which is not extended-$\Cap$-shaped can be path-like, and illustrates the way of extending a GRT into a tree-like structure with finite-length interfaces constituting a connected graph without cycles (i.e., a structure without bounded grains).

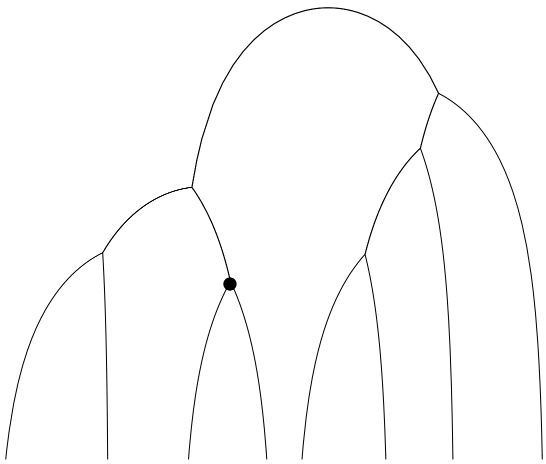

Figure 11: A tree-like structure. If the junction marked by the disk in is removed, the GRT is based on a path of junctions.

Clearly, adding new junctions to unbounded inner interfaces is strongly limited. In particular, in the case of UBM, asymptotes of interfaces are distributed at the steps of $w/3$. One cannot add a new junction on an inner interface sharing its asymptote with another interface as this would lead to interface intersection. This is illustrated in Fig. 12.

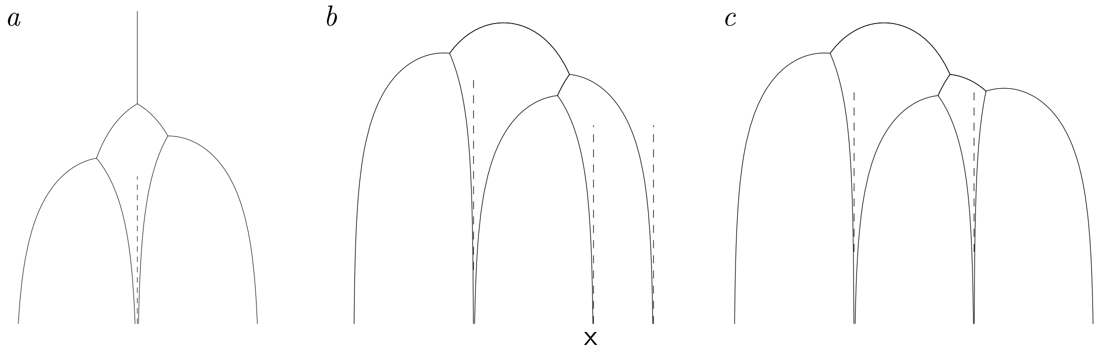

Figure 12: GRTs illustrating vanishing of asymptotic cell widths in the case of UBM networks. (*a*) GRT with Y-shaped triod. The width of the cell with this triod is zero. (*b*) A path-based network. (*c*) A tree-like network. A new junction cannot be added to any unbounded inner interface except the one marked by x in (*b*).

Structures with bounded cells

More complicated configurations contain bounded cells. A basic feature of bounded cells follows again from the property (5) of intersecting GRs. Let the vertices of an N-sided bounded cell be numbered by n, and let ϕ_n be the internal angle at vertex (n). With the curvature $\kappa_n = \pi - \phi_n$ concentrated at the vertex, and the curvature integrated over boundaries of the cell equal to zero, one has the closing condition $2\pi = \sum \kappa_n + 0$ or

$$\sum_{n=1}^{N} \phi_n = (N-2)\,\pi \ , \tag{14}$$

i.e., the same formula as that for the sum of interior angles of an N-sided polygon. This is in agreement with the rule for the rate $\dot{A}$ of change of cell area applicable in the case of cells with boundaries migrating by curvature and arbitrary angles at triple-points

$$\dot{A} \propto (N-2)\,\pi - \sum_{n=1}^{N} \phi_n \ .$$

In view of (14), the area A of the cell built of GRs remains unchanged as expected for steady (i.e., also area-preserving) flow of the network. Example networks with single bounded cells are shown in Fig. 13. Clearly, one may consider GRTs with multiple bounded cells; an example is shown in Fig. 14.

If the angles at triple points are $\phi_n = 2\pi/3$, then eq.(14) implies that $N = 6$. This agrees with the classic Mullins extension of the von Neumann's law: within UBM, the area of a bounded cell is preserved if and only if the cell is six-sided [20].

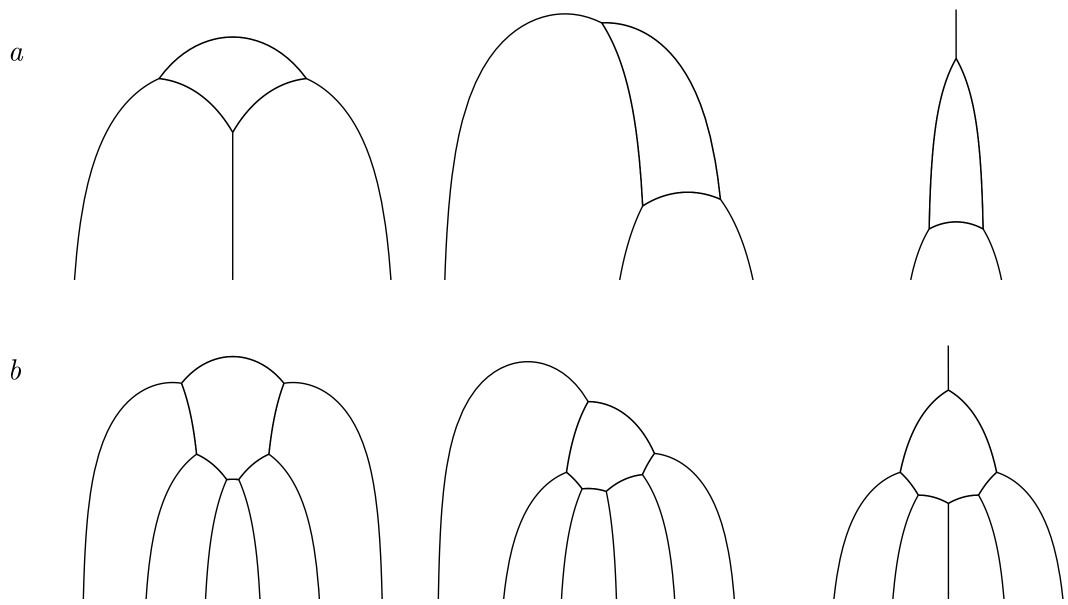

Figure 13: Example bounded cells. (a) "Triangular" equi-angle configurations. The internal angles of the bounded cells are $\pi/3$ and all remaining angles between interfaces are $5\pi/6$. (b) Six-sided equi-angle UBM configurations. All angles are $2\pi/3$.

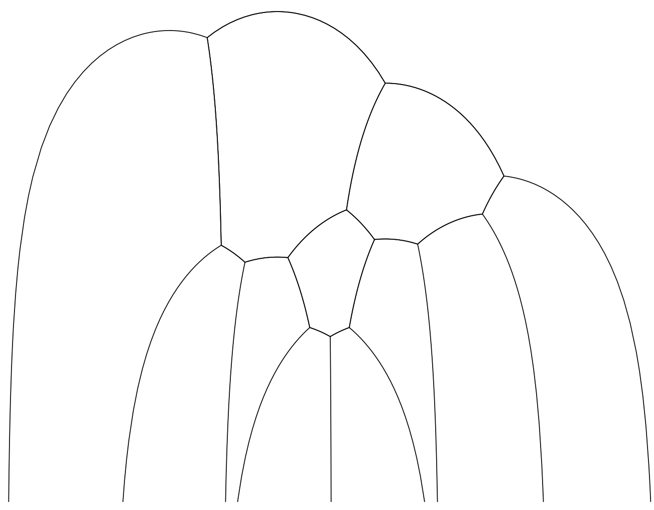

Figure 14: Example GRT with three six-sided UBM cells. It was built by adding new cells to the asymmetric GRT of Fig. $13b$. All angles are $2\pi/3$.

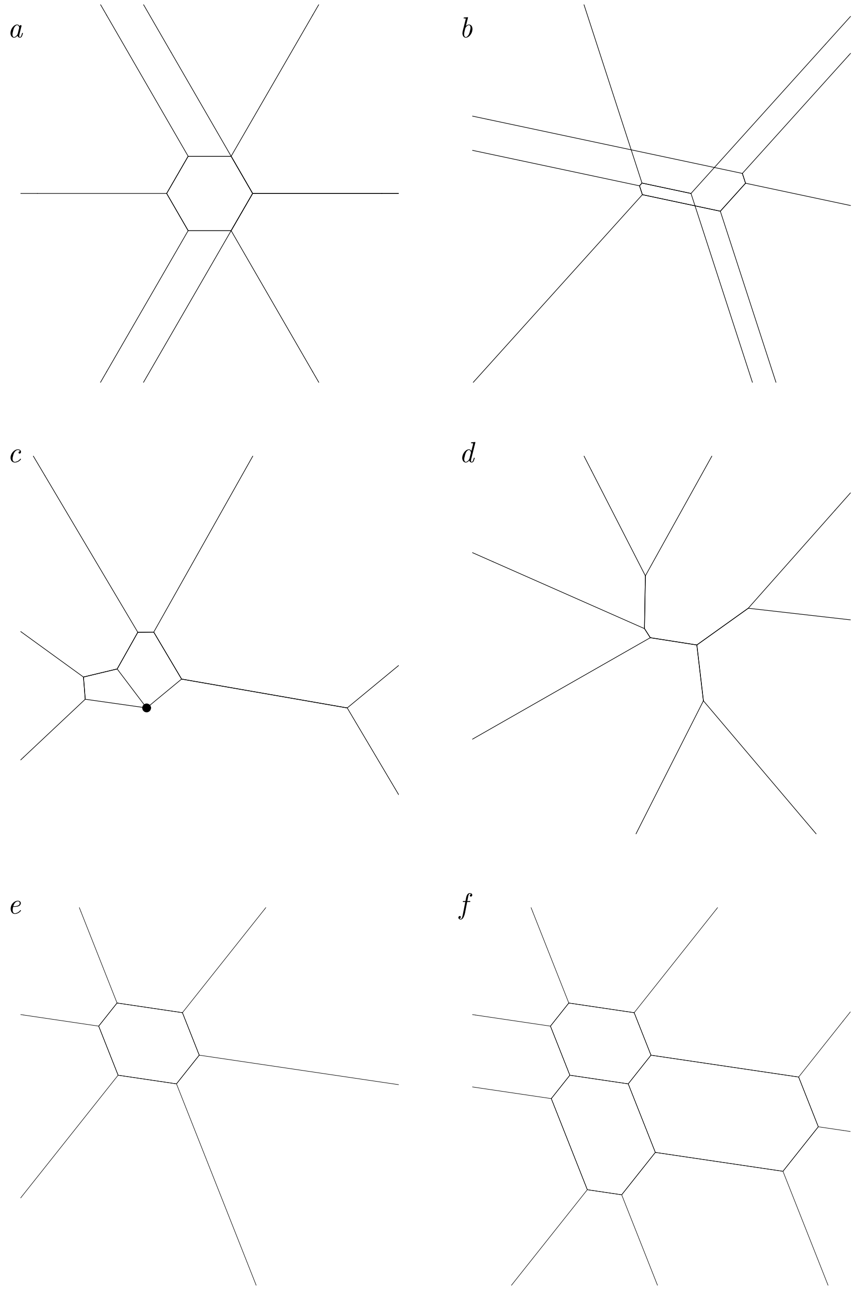

Figure 15: Images of GRTs transformed to (x', y') coordinates. They correspond to networks shown in Fig. 9*a* (*a*), Fig. 9*b* (*b*), Fig. 10 (*c*), Fig. 11 (*d*), the middle structure of Fig. 13*b* (*e*) and Fig. 14 (*f*). In (*c*), the segments meeting at the point $(x', y') = (0, 0)$ marked by disk correspond to the (directed up) half-lines of the network. All angles in (*a*), (*b*), (*e*) and (*f*) are $2\pi/3$.

Another way of constructing GRTs

The networks above were described by Cartesian coordinates (x, y) of points of interfaces. GR curves andl lines translating along $-y$, after transformation to

$$(x', y') = \exp(-cy)\ (\cos(cx), \sin(cx)) \tag{15}$$

become straight lines. With complex numbers $z = x+iy$ and $z' = x'+iy'$, the transformation (15) has the form $z' = \exp(icz)$. Since the function $z' = z'(z)$ is holomorphic and its derivative is non-zero on the whole complex plane, the transformation is conformal on the plane. It transforms GRTs to complexes of polygons and half-lines meeting at the same angles as the corresponding interfaces (Fig. 15). Images of upper unbounded interfaces of a GRT meet at the origin of the complex plane and those of lower unbounded interfaces extend to complex infinity. It is easy to see that if a network is translated along y by t_y, its image is scaled by $\exp(-ct_y)$. Translation along x by t_x results in rotation of the image about the origin $(x', y') = (0, 0)$ by ct_x. The function $\exp(icz)$ is periodic with the period $2\pi/c = 2w$, i.e., for given y, points spaced by $2w$ along x are all mapped to the same z'. In effect, mapping of wide structures leads to overlappings (Fig. 15a) and intersections (Fig. 15b) of interface images.

The transformation

$$(x, y) = c^{-1}\left(\arctan(x', y'),\ -\log\sqrt{x'^2 + y'^2}\right)\ , \tag{16}$$

inverse to (15) can be used to get translating networks from complexes of polygons and half-lines.[3] It is easy to see that the resulting structure depends on the location of the complex in the reference frame; this is illustrated in Fig. 16. Clearly, not every complex of polygons and half-lines will lead to a sensible translating network of interfaces. No segment or half-line can cross the negative real axis ($y' = 0$ and $x' < 0$). The shorter form

$$z = -ic^{-1}\log(z')$$

of the inverse transformation (16) indicates that a natural setting for constructing translating networks from suitably designed complexes is the Riemann surface of the multivalued log function. Overlapping parts of complexes need to be mapped on different sheets of the surface. This method of constructing translating networks based on conformal transformation is easy to implement and more elegant than the brute-force approach of section 3, but it is limited to the case of $M = 0$ (equal widths of GRs). It is also worth noting

[3]The function arctan at (x', y') gives the principal value of the argument of $z' = x' + iy'$, its codomain is $(-\pi, \pi]$, and it is indeterminate at $(0, 0)$.

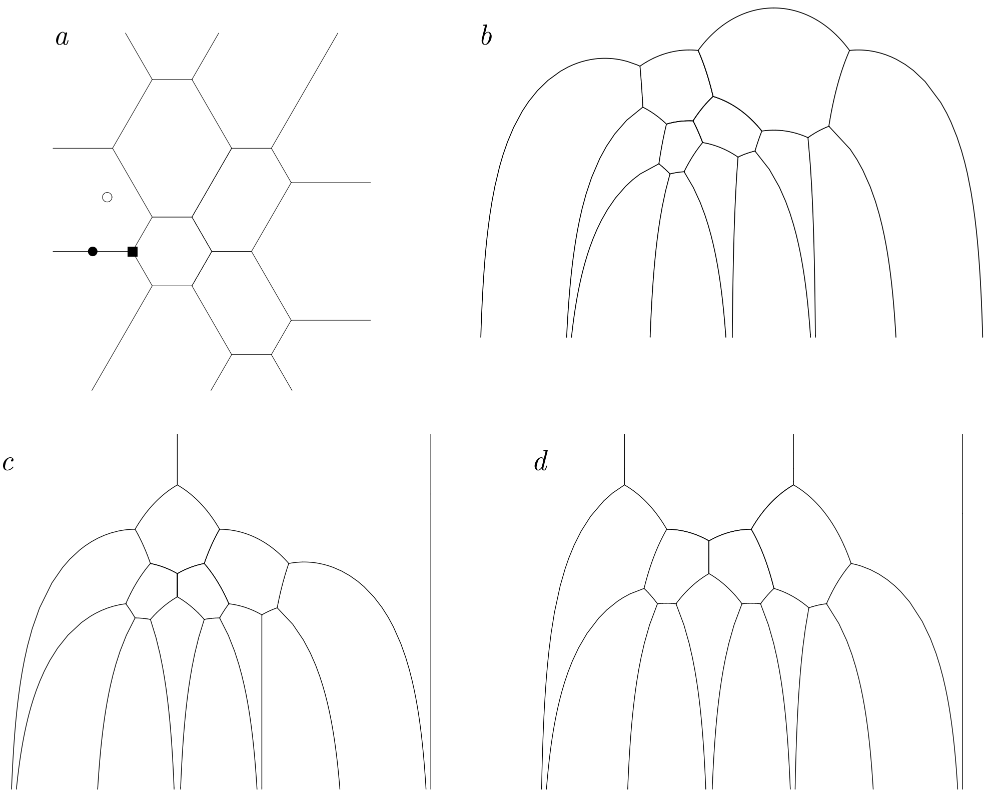

Figure 16: Example complex of of hexagons and half-lines with the angles of $2\pi/3$ (a) and three GRTs obtained by transformation (16). The one shown in (b) is obtained when the origin of the (x', y') reference frame is at the point marked by circle, (c) corresponds to the point marked by disk, and (d) corresponds to square. In (c) and (d), the complex is mapped on a GRT and a disconnected line.

that the representation by complexes of polygons and half-lines on the complex plane can be a step toward a more complete characterization of the translating networks. By inverse stereographic projection of the plane, one gets simple geometry of images of unbounded interfaces; they meet at the poles of the sphere (Fig. 17). Such projections can be also be obtained directly form (x, y) coordinates using

$$(x_s, y_s, z_s) = (\mathrm{sech}(cy)\ \cos(cx),\ \mathrm{sech}(cy)\ \sin(cx),\ -\tanh(cy))\ , \tag{17}$$

where (x_s, y_s, z_s) are Cartesian coordinates of points on the unit sphere. In the case of UBM-based translating networks, images of unbounded interfaces on the sphere meet at the angles being multiples of $\pi/3$.

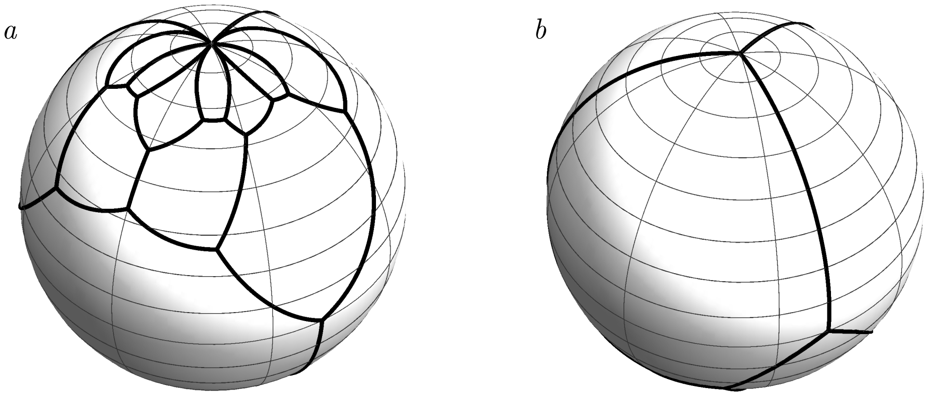

Figure 17: Projection (17) of the structure shown in Fig. 16d on sphere (or stereographic projection of the complex plane of Fig. 16a with the origin marked by square). (a) View on the pole which is the meeting point of lower unbounded interfaces of Fig. 16d (or the complex infinity). (b) View on the pole which is the meeting point of upper unbounded interfaces (or projection of the origin of the complex plane).

5. Concluding remarks

The paper describes construction of translating interface networks applicable in verification of algorithms and testing of computer codes for simulation of capillarity-driven boundary migration during grain growth in polycrystalline materials. The networks are built of pieces of half-lines and Grim Reapers meeting at triple junctions at angles determined by equilibrium conditions. The construction is described for the principal case ($M = 1$) with interface tensions influencing the speed of migration and equilibrium angles. Interesting properties arise in more specific situations: first, when all GRs are of the same width ($M = 0$), and second, in the case of UBM when all GRs are of the same width, and all angles are $2\pi/3$ (σ = const). The equality of GR widths, makes it possible to construct translating networks by a conformal mapping of properly arranged complexes of polygons and half-lines with triple points. Moreover, there are simple relationships between cell dimensions and angles at triple junctions, and simple expressions for the rates of areas swept by the networks.

The construction and detailed understanding of properties of theoretically solvable models is essential for identifying strengths and deficiencies of grain growth simulation algorithms and software. Besides the curvature-driven migration mode, the grain growth simulations must deal with other aspects of the phenomenon, in particular, with its 3D character, anisotropy of the interface energy, variability of interface mobilities, topological changes, et cetera. These issues are beyond the scope of this paper. Let us only note that the 2D translating networks are not easily generalizable to 3D (e.g., [22]), but – in principle – 3D

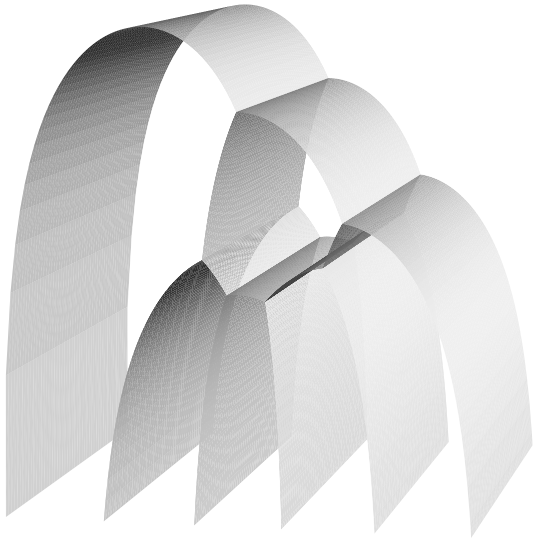

Figure 18: Schematic of the cylinder over one of the GRTs of Fig. 13*b*.

simulations can be tested using cylinders over the GRTs (Fig. 18). Specimens used in junction-drag experiments and boundary mobility measurements [10–12] had the form of cylinders over Y-shaped triods.

With verification of algorithms and testing of simulation codes in mind, there is a question of stability of the analytical translating networks to perturbations. The answer will depend on the character of perturbations, but some results indicate stability in relatively general settings; see, e.g, the analysis of Y-shaped GRTs (named "equal-order grain boundary model") in [23]. Assuming stability, the simplest approach to testing would be to start a simulation using an analytically obtained translating boundary network and check whether the simulated structure does move by translation. An ideal simulation code would deal with arbitrary translating network. In practice, after large time increments, real programs will fail to preserve complicated structures. One may devise measures of the quality of imitating the curvature driven migration by quantifying deviations from a chosen exact steady network. They can be based on measures for the dissimilarity of figures (like Fréchet or Hausdorff distances, e.g., [24]).

The extension of the catalog of translating configurations and knowledge on their properties can be also useful for designing grain growth related experiments. With the development of sophisticated crystallization techniques (e.g., [25, 26]), better understanding of steady-state networks can help devising new configurations for measurements of physical properties of boundaries.

References

[1] M.A. Miodownik. A review of microstructural computer models used to simulate grain growth and recrystallisation in aluminium alloys. *J. Light Met.*, 2:125–135, 2002.

[2] H.V. Atkinson. Theories of normal grain growth in pure single phase systems. *Acta Metall.*, 36:469–491, 1988.

[3] H. Garcke, B. Nestler, and B. Stoth. A multiphase field concept: numerical simulations of moving phase boundaries and multiple junctions. *SIAM J. Appl. Math.*, 60:295–315, 1999.

[4] S. Esedoḡlu and F. Otto. Threshold dynamics for networks with arbitrary surface tensions. *Commun. Pur. Appl. Math.*, 68:808–864, 2015.

[5] Y. Jin, N. Bozzolo, A.D. Rollett, and M. Bernacki. 2D finite element modeling of misorientation dependent anisotropic grain growth in polycrystalline materials: Level set versus multi-phase-field method. *Comput. Mater. Sci.*, 104:108–123, 2015.

[6] M. Elsey, S. Esedoḡlu, and P. Smereka. Diffusion generated motion for grain growth in two and three dimensions. *J. Comput. Phys.*, 228:8015–8033, 2009.

[7] S. Esedoḡlu, S. Ruuth, and R. Tsai. Diffusion generated motion using signed distance functions. *J. Comput. Phys.*, 229:1017–1042, 2010.

[8] S. Cox and G. Mishuris. Remarks on the accuracy of algorithms for motion by mean curvature in bounded domains. *J. Mech. Mater. Struct.*, 4:1555–1572, 2009.

[9] C. Dunn, F. Daniels, and M. Bolton. On the problem of grain boundary movement. *Trans. AIME*, 185:708–709, 1949.

[10] D.A. Molodov, T. Gorkaya, C. Günster, and G. Gottstein. Migration of specific planar grain boundaries in bicrystals: application of magnetic fields and mechanical stresses. *Front. Mater. Sci. China*, 4:291–305, 2010.

[11] G. Gottstein and L.S. Shvindlerman. *Grain Boundary Migration in Metals: Thermodynamics, Kinetics, Applications*. CRC Press LLC, Boca Raton, FL, USA, 1999.

[12] U. Czubayko, V.G. Sursaeva, G. Gottstein, and L.S. Shvindlerman. Influence of triple junctions on grain boundary motion. *Acta Mater.*, 46:5863–5871, 1998.

[13] H.P. Halldorsson. Self-similar solutions to the curve shortening flow. *Trans. Amer. Math. Soc.*, 364:5285–5309, 2012.

[14] C. Mantegazza. Evolution by curvature of networks of curves in the plane. In P. Baird, A. El Soufi, A. Fardoun, and R. Regbaoui, editors, *Variational Problems in Riemannian Geometry: Bubbles, Scans and Geometric Flows*, pages 95–109. Springer, Basel, 2004.

[15] C. Mantegazza, M. Novaga, and A. Pluda. Motion by curvature of networks with two triple junctions. *Geom. Flows*, 2:18–48, 2016.

[16] V.E. Fradkov and D. Udler. 2D normal grain growth: topological aspects. *Adv. Phys.*, 43:739–789, 1994.

[17] R. Shuttleworth. The surface tension of solids. *Proc. Phys. Soc. A*, 63:444–457, 1950.

[18] T.D. Gurkov and P.A. Kralchevsky. Surface tension and surface energy of curved interfaces and membranes. *Colloid. Surface.*, 47:45–68, 1990.

[19] A.V. Galina, V.E. Fradkov, and L.S. Shvindlerman. Vliyanie podvizhnosti trojnogo styka zieren na migratsiu granits. *Fiz. Metal. Metalloved.*, 63 (6):1120–1122, 1987.

[20] W. W. Mullins. Two-dimensional motion of idealized grain boundaries. *J. Appl. Phys.*, 27:900–904, 1956.

[21] M.A. Grayson. The heat equation shrinks embedded plane curves to round points. *J. Differ. Geom.*, 26:285–314, 1987.

[22] S.J. Altschuler and L.F. Wu. Translating surfaces of the non-parametric mean curvature flow with prescribed contact angle. *Calc. Var.*, 2:101–111, 1994.

[23] M. Beck, Z. Pan, and B. Wetton. Stability of travelling wave solutions for coupled surface and grain boundary motion. *Physica D*, 239:1730–1740, 2010.

[24] A. Dumitrescu and G. Rote. On the Fréchet distance of a set of curves. In *Proceedings of the 16th Canadian Conference on Computational Geometry, CCCG'04*, pages 162–165, Concordia University, Montréal, Canada, 2004.

[25] P. Lejček, J. Kopeček, and M. Jarošová. Growth of oriented tricrystals of an Fe-Si alloy. *J. Crys. Growth*, 287:262–266, 2006.

[26] L.G. Ware, D.H. Suzuki, K.R. Wicker, and Z.C. Cordero. Grain boundary plane manipulation in directionally solidified bicrystals and tricrystals. *Scripta Mater.*, 152:98–101, 2018.